Applied Thermal Engineering 239 (2024) 122122

Contents lists available at ScienceDirect

Applied Thermal Engineering

journal homepage: www.elsevier.com/locate/apthermeng

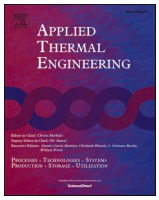

Research Paper

Experimental evaluation of direct-to-chip cold plate liquid cooling for high-heat-density data centers

Ali Heydari [b], Ahmad R. Gharaibeh [a,*], Mohammad Tradat [b], Qusai soud [a], Yaman Manaserh [b], Vahideh Radmard [b], Bahareh Eslami [b], Jeremy Rodriguez [b], Bahgat Sammakia [a]

[a] Department of Mechanical Engineering, ES2 Center, Binghamton University-SUNY, NY, USA
[b] NVIDIA Corp., Santa Clara, CA, USA

ARTICLE INFO

Keywords:
Data centers
Thermal management
High power density racks
Liquid cooling
CDU

ABSTRACT

Owing to the dramatic increase in IT power density and energy consumption, the data center (DC) sector has started adopting thermally- and energy-efficient liquid cooling methods. This study examines a single-phase direct-to-chip liquid cooling approach for three high-heat-density racks, utilizing two liquid-to-air (L2A) cooled coolant distribution units (CDUs) and a combined total heat load of 128 kW. An experimental setup was developed to test different types of CDUs, cooling loops, and thermal testing vehicles (TTVs) for different operating conditions. IR images and the collected data were used to investigate the effect of air recirculation between cold and hot aisle containments on the CDU's performance and stability of supply air temperature (SAT). Three different types of cooling loops (X, Y, and Z) were characterized thermally and hydraulically. Results show that Type Y has the lowest cold plate thermal resistance and pressure drop, among others. In a later test that included a single rack at a heat load of 53 kW and a single CDU, the heat capture ratio for fluid was found to be 94%. Experiments show that using blanking panels on the back of the racks limits hot air recirculation and maintains a steady SAT in the cold aisle. Finally, the CDU performance was evaluated at a high heat load for the three racks at 128 kW, and the average cooling capacity of the units is 58.6 kW, and the effectiveness values for CDU 1 and CDU 2 are 0.83 and 0.82, respectively.

1. Introduction

Artificial intelligence is a growing field that has the potential to have a big influence on everyone's daily lives. Deep learning, machine learning, and big data may require a substantial amount of computational power and computing resources in the era of artificial intelligence. This suggests that a large number of high-performance processors, including high-performance central processing units (CPUs), graphics processing units (GPUs), field-programmable gate arrays (FPGAs), and application-specific integrated circuit (ASIC) devices, may be required. Most recent advancements combine many of them into a single server or compute cluster to maximize performance and provide additional functionality to data processing and telecommunications equipment while keeping the total space occupied the same. However, this packaging will result in a significant increase in power density. The maximum power for a conventional air-cooled data center is 20–30 kW per rack; however, liquid cooling can push that up to 100 kW [1].

In traditional data centers, the mainstays of data center cooling are air-cooled systems. However, they are close to their cooling capacity limits, particularly when a cluster of racks is completely filled with nodes that require a lot of computational power [2–4]. To improve cooling efficiency and efficiently dissipate a significant amount of heat produced by high-performance processors, novel and more efficient cooling methods are being deployed independently of or in conjunction with traditional air-cooling systems [5]. For example, approaches like indirect single- or two-phase liquid cooling employing microchannel cold plates, as well as fully submerged direct liquid-cooled technology, have been reported. [6–13]. Older data centers lack higher floors, have restricted access to chilled water supplies, and have confined air distribution paths, which make it difficult to use single-phase cooling methods. Liquid-to-air (L2A) cooling distribution units (CDUs) of different types, such as in-rack, in-row, rear door, and side car [14–17], which circulate liquid coolant within cooling loops positioned atop each server, have therefore come to be recognized as a method for successfully cooling servers. These CDUs allow for the efficient transfer of heat by pumping cold liquid into the cooling loops connected to the servers or chips and then returning warm liquid to the CDU heat exchanger (HX).

* Corresponding author.
E-mail address: agharai1@binghamton.edu (A.R. Gharaibeh).

https://doi.org/10.1016/j.applthermaleng.2023.122122
Received 3 September 2023; Received in revised form 2 November 2023; Accepted 27 November 2023
Available online 30 November 2023

Nomenclature

ρ	Fluid density
q	Heat flow rate
C_p	Specific heat
Q	Volumetric flow rate
T	Temperature
$\dot{m}$	Mass flow rate
ε	Heat exchanger effectiveness
R_{th}	Thermal resistance
P	Pressure
ΔP	Pressure drop
ω_R	Uncertainty

Abbreviations

CFD	Computational Fluid Dynamics
CDU	Coolant distribution unit
CRAH	Computer Room Air Handler
DC	Data center
TTV	Thermal testing vehicle
L2A	Liquid-to-air
HX	Heat exchanger
CL	Cooling loop
CC	Cooling capacity
SAT	Supply air temperature
RAT	Return air temperature
SFT	Supply fluid temperature
RFT	Return fluid temperature
ITE	Information technology equipment
GPU	Graphics processing unit
CV	Control valve

Subscripts

B	Buoyancy force
liq	Liquid
in	Inlet
out	Outlet
PG	Propylene Glycol

The heat is subsequently removed using cold air utilizing fans in a HX.

Gao [18] experimentally characterized a technology cooling system loop (TCS) in a liquid cooling system for servers. Various operation scenarios were investigated, including coolant flow rates, supply temperatures, and air velocities. Moreover, the control system response to dynamic changes in the operation is also presented and judged based on the speed and accuracy of delivering the desired operating conditions. Mohamad [19] created and evaluated an innovative liquid cooling architecture for IT racks in OVH cloud data centers (DCs). The study compared three alternative heat rejection devices under four climate conditions in a performance assessment of a 600-kW data center. In Schmidt's study [15], an air-to-liquid heat exchanger (A2L HX) was mounted on the side of a server cabinet to reduce the negative effects of hot air recirculation. The A2LHX prevented the recirculation of hot air and helped maintain stable flow and temperature levels for the other components by removing the server's 35-kW heat load. Data center efficiency is crucial for minimizing costs, reducing environmental impact, and ensuring reliable operations in an increasingly data-dependent world. In a hybrid cooling technique for DCs, Udakeri [20] suggested that combining liquid cooling and air cooling could be very efficient. In a more generalized study, Capozzoli [21] discussed and compared the existing and emerging cooling technologies for data center applications. The pros and cons of each technology were highlighted, along with a thorough look at future technologies. Various conclusions were summarized, such as the importance of using waste heat recovery techniques and integrating renewable energy sources (RES) and thermal energy sources (TES). Moreover, the value of implementing energy efficiency measures was also highlighted, such as aisle containment, optimizing air distribution, and reducing active mechanical equipment usage. Recent studies have focused more on the technicalities of cooling system employment. An in-depth investigation by Shahi [22] aimed at showing the effect of flow variation on the cooling performance of a server-level liquid cooling system. The performance indicators included the core temperature, memory module temperatures (DIMM), and the temperature of the platform controller hub (PCH). Various power levels were tested, along with several inlet temperatures for the coolant. It was shown that the effect of increasing the coolant flow rate is more obvious at 0–50% of the total thermal load, whereas the significance of this parameter becomes less in the range of 50–100% of the total thermal load of the server. Nada [23] looked at the thermal and hydraulic efficiency of servers' liquid cooling systems. Different cooling fluid path designs, including parallel and serpentine arrangements, as well as various geometrical dimensions, were researched under a variety of operating scenarios.

Liquid cooling systems operating at elevated supply fluid temperatures can achieve higher efficiency levels, reduced cooling system complexity, enhanced equipment reliability, and the potential to utilize waste heat for other purposes. Iyengar [24] experimentally studied hybrid cooling at rack level. The study incorporated cooling for low-power devices and liquid cooling for higher-power devices at high coolant supply temperatures. This type of server could accept higher coolant inlet temperatures for water up to 45 °C and air up to 50 °C, and it reduced overall energy consumption by 25%. Zimmermann [25] demonstrated that hot water can serve as a coolant to address the cooling requirements of data centers, utilizing insights gained from an experimental data center prototype named Aquasar. Furthermore, according to the authors, up to 80% of the DC waste heat can be recovered when warm water is reused for space heating. In the same concept, Iyengar [26] studied the performance of a novel high-temperature liquid cooling system based on the economizer concept. The authors documented their efforts in developing chiller-less, liquid-cooled systems for energy-efficient data centers and thermal management. A 15-kW rack with liquid-cooled servers was used for that research, with coolant temperatures up to 45 °C. An energy savings of around 30% was anticipated using the proposed warm coolant system. Another study conducted by Rubenstein [27] proposed a cooling approach that relies on warm water for electronics cooling instead of chilled coolant. The effects of various environmental conditions on the system's performance are documented, along with an analytical model describing the heat transfer within the system. The results showed that up to 50% savings in the total energy consumption of the cooling system can be achieved using the proposed approach.

Hwang [28] developed an energy use model for data center thermal management based on conventional air-cooling systems and hybrid cooling. The proposed model was validated experimentally for rack-level thermal management. Various parameters affecting energy usage were considered for air and hybrid cooling schemes. It was concluded that the air-cooling system is less dependent on the ambient air temperature than the hybrid cooling system. On the other hand, the hybrid cooling system resolves most of the limitations associated with air cooling. It also shows enhanced energy performance because of the reduction in the amount of cooling required by air-cooled auxiliary components. Another example is the research done by Watson [29], which conducted a CFD analysis for air-cooling systems with contained hot aisles and liquid-cooled immersion systems. ANSYS Fluent was used to predict the performance of each system while the rack power density

was changed from 15 kW to 30 kW. The immersion cooling system was able to maintain a 25 °C outlet temperature for all experimented power levels, while the air-cooling system showed an increase of 18 °C in the coolant outlet temperature. The most recent paper in this field was by Heydari [30], who experimentally and numerically studied the performance of liquid-to-liquid CDUs under various operation conditions in air-cooled DCs.

This study focuses on developing and testing a direct-to-chip cold plate liquid cooling system for high-heat-density data centers, aiming to enhance cooling efficiency and energy performance. The experimental setup used in-row CDUs with an L2A HX. This system supplies chilled liquid to cold plates that are attached to high heat-density heaters intended to mimic the constant heat flux produced by processors. Then the hot air is immediately vented from the heat exchanger into a hot aisle containment. The setup includes different kinds of cooling loops, rack manifolds, and thermal testing vehicles (TTVs). Full descriptions of system components, the best practices in handling them, and the performance of each cooling loop in terms of thermal resistance and pressure drop appear below, and the CDU's response at full heat load is analyzed and summarized in this paper. Notably, this paper signifies a notable gap in the existing body of research, as there is a lack of substantial large-scale experimental demonstrations of a deployed single-phase liquid cooling approach in data centers. The majority of the existing literature primarily focuses on thermal management at the chip, server, and low load rack levels. Our investigation reveals the adaptability of liquid cooling design to achieve an impressive 52 kW per rack, signifying a substantial departure from prevailing air-cooling methodologies. By enhancing comprehension of liquid cooling's efficacy in augmenting cooling and energy efficiency, cooling capacity, and equipment reliability for high-power density racks within data centers, this work assumes paramount importance.

2. Experimental setup

2.1. Setup Description

The experimental setup consists of three racks and two identical in-row L2A CDUs, as seen in Fig. 1. Both CDUs are liquid-to-air heat exchangers that operate in the constant flow rate mode and have a cooling capacity of 63 kW. Each rack is loaded with five thermal testing vehicles

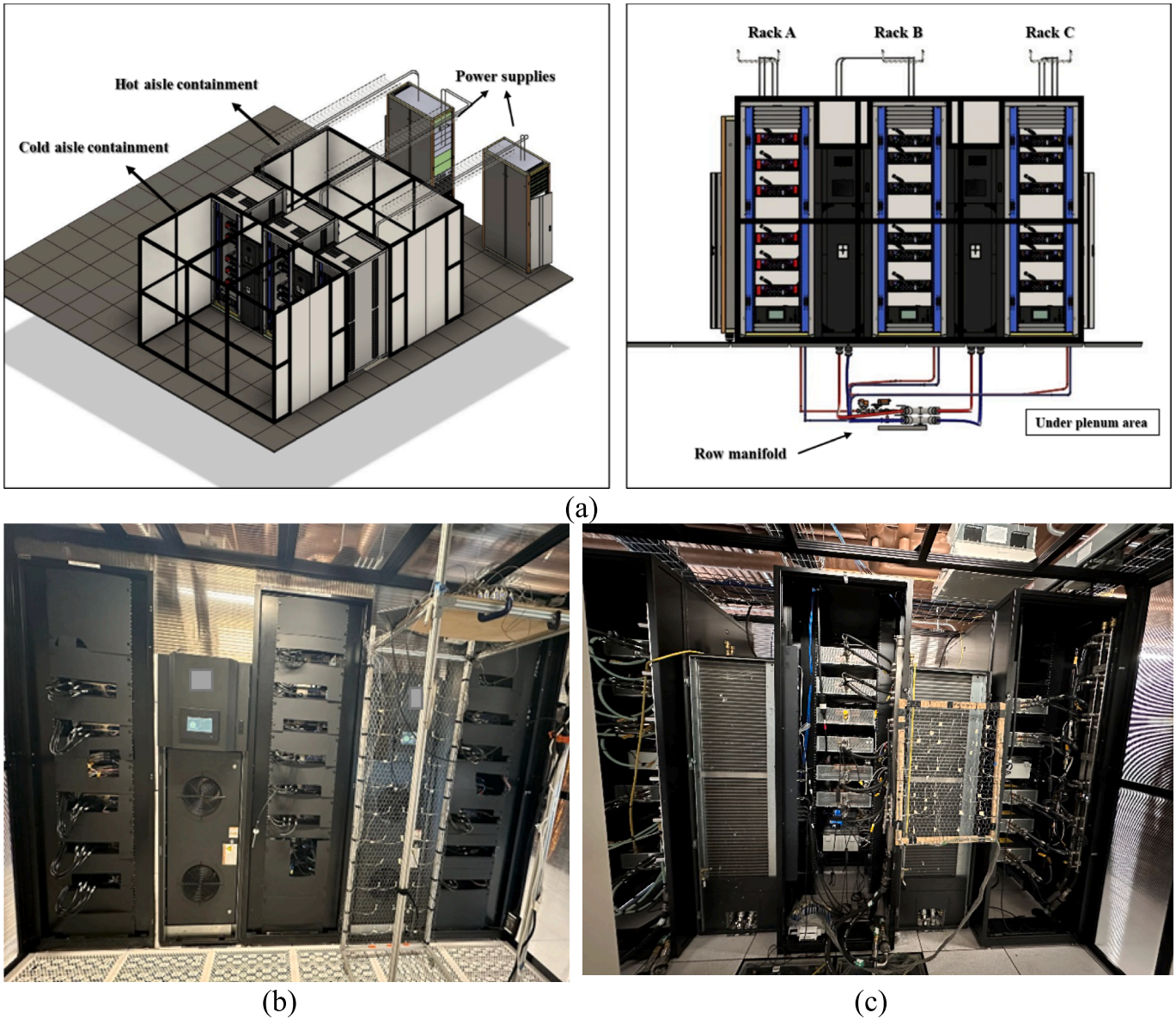

Fig. 1. (a) CAD drawing of the experimental setup. (b) Back view of the experimental setup. (c) Front view of the experimental setup.

(TTVs) that consist of eight big heaters and six small heaters with a T-type thermocouple installed in each one to measure their temperature. Each TTV can reach a total power of 9.2 kW (1 kW/big heater and 200 W/small heaters). Each CDU has two fans and two pumps; one of the pumps is redundant. The heat exchanger uses the cold air supplied by two computer room air handler units (CRAH) through raised floor perforated tiles as the primary side, while it pumps a propylene glycol mixture with water (PG 25) as the secondary side to the racks. The PG25 was supplied from the CDUs to the rack manifold via the row manifold, and on the return side of the row manifold from each rack, control valves were installed and utilized to manage and assure appropriate flow through every rack as well as to gather flow data, including coolant temperature, glycol percentage, and flow rate. In this setup, three custom rack manifold designs A, B, and C with six pairs of quick disconnect ports are placed vertically on the rack. Efficient and easy coupling between the rack manifold and the row manifold is achieved through the utilization of streamlined FD83 quick disconnects. Schrader air pocket release valves at the top of each rack manifold eliminate trapped air or bubbles that would cause excess pressure differentials and might damage the CDU pumps. Additional details on the experimental setup can be found in [31,32].

The inlet and outlet manifolds between the rack manifold and cooling loops were instrumented with ultrasonic flow meters, pressure sensors, and temperature sensors to measure the cooling loop flow rate, pressure drop, and coolant inlet and outlet temperatures, as seen in Fig. 2.

Table 1 provides a summary of instrumentation models and specifications used in the experiment.

Table 1
Specifications of experimental apparatus.

Description	Specification	Accuracy
Airflow rate	Flow hood multimeter (ADM-850 L).	± 3% of reading
Fluid flow rate	FD-X A1 clamp-on micro flow sensor.	±0.003 ml/min
Data acquisition system	KEYSIGHT DAQ970A	–
Raised floor tiles	Perforated tiles with an open area of 32%.	–
Pressure readings	KEYENCE GP-M001T (–14.50 to 14.50 PSI) KEYENCE GP-M010T (–14.5 to 145 PSI) .	±1% of full scale or less.
Power supply	Keysight PS-XHW-200	±0.1%
Air temperature	DegreeC / Cambridge AccuSense ATM2400 airflow temperature monitor.	±0.2 °C
IR images	FLIR E4 Thermal imaging camera with a temperature range of −20 to 250 °C.	0.15 °C thermal sensitivity

2.2. Thermal testing vehicle design

To replicate the thermal properties of a server, thermal equipment called a thermal testing vehicle (TTV) with uniform heat flux heaters was loaded into the racks in a 3U chassis, as shown in Fig. 3(a). The TTV, which mimics a real high-heat-density device, is an affordable and ideal option to assess the thermal performance of the proposed cooling loops for servers. Two heaters with different geometries were used to evaluate two different processors (GPUs and NV Switches). Each TTV consists of 8 big heaters (Type A), each with a size of 50.8 mm × 50.8 mm × 6.23 mm and an electrical resistance of 48.4 Ω ± 5%, and 6 small heaters (Type B) with a size of 25.4 mm × 25.4 mm × 5.4 mm and an electrical resistance of 242 Ω ± 5%, with a T-type thermocouple installed in each to measure the top surface temperature. A Type A heater can reach a maximum power of 1000 W, while a Type B heater can reach 200 W. The total power level a TTV can reach is 9.2 kW.

2.3. Cooling loops design

This experiment employed three distinct cooling loops, illustrated in Fig. 4. TTVs in the same rack were attached to the same type of cooling loops. Rack A has cooling loops X, Rack B has cooling loops Y, and Rack C has cooling loops Z. Each cooling loop has a unique flow distribution, for instance; in cooling loop X, as seen in Fig. 4 (a), the coolant enters the large cold plates attached to heaters 2 and 4 at the same time and then flows to 1 and 3, where they receive the pre-heated coolant, and then exits the cooling loop through the common hose. In the same way, the coolant enters the large cold plates attached to heaters 5 and 7, then enters heaters 6 and 8 as pre-heated coolant, and then exits the cooling loop. For the small cold plates attached to Type B heaters, the fluid enters cold plate 1, moves to 2, and from there to cold plate 3 before exiting the cooling loop, and the same for cold plates 6 to 5, and 4. Cooling loop Y (Fig. 4(b)) shares the same fluid distribution in the small cold plates side as in cooling loop X, while it's different in the large cold plates side, where the even-numbered cold plates receive the fluid first, after which it travels through the odd-numbered cold plates and exits the cooling loop. In cooling loop Z (Fig. 4(c)), only the small cold plates 2 and 5 receive fresh fluid, and then the fluid splits from 2 to 1 and 3, and the pre-heated fluid distributes to the large cold plates 1 and 3, and from

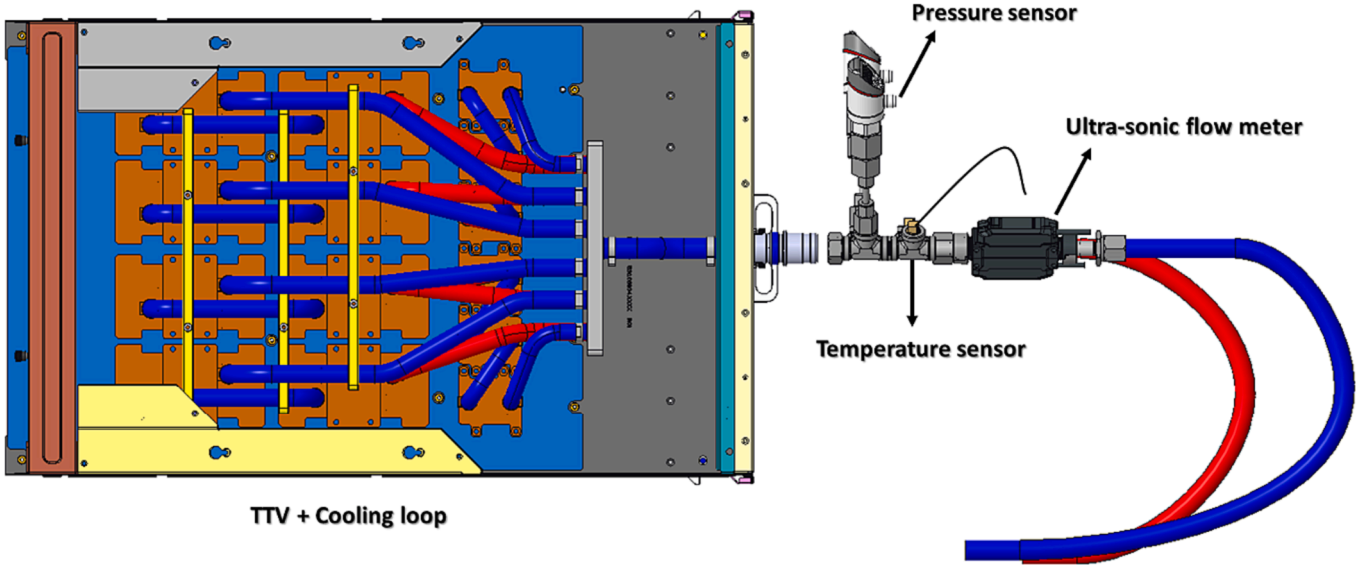

Fig. 2. CAD model for the instrumented manifold that connects the rack manifold with the cooling loop attached to the TTV.

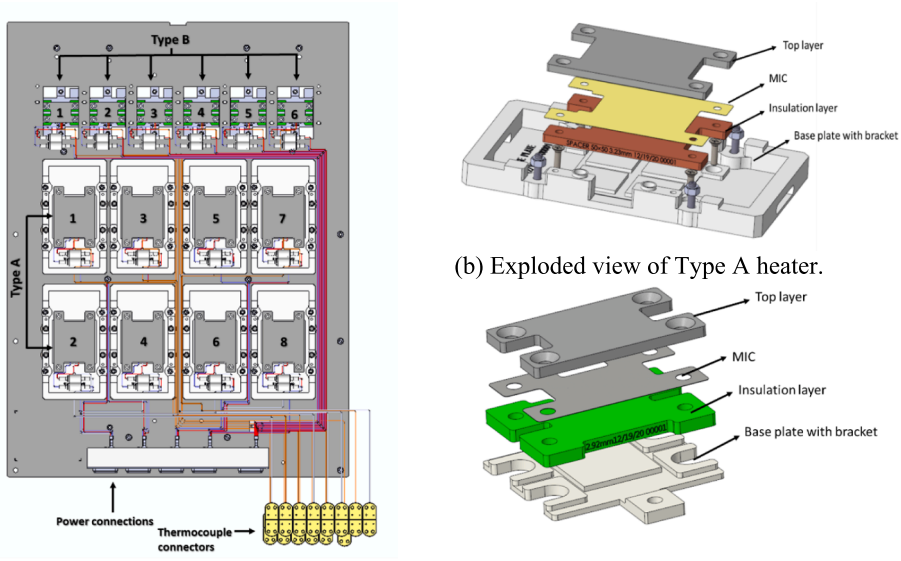

(a) TTV used in the racks.

(b) Exploded view of Type A heater.

(c) Exploded view of Type B heater.

Fig. 3. CAD model for the TTVs used in the experiment with an exploded view for the heaters.

them to 2 and 4, and then exits the cooling loop. The remaining small and large cold plates follow a similar pattern before the fluid finally leaves the cooling loop.

3. Results and discussion

3.1. Thermal and hydraulic performance of cooling loops

A rack-level experimental setup was used to characterize the pressure drop for each cooling loop and the thermal resistance for the larger cold plates in each of the three types of cooling loops. For the thermal test of single A-type heater cold plates, it was conducted under different flow rates; the Type A heater power was 550 W, and the supplied fluid temperature was 32 °C with PTM 7900 phase change thermal interface material (TIM) between the heater and the cold plate. Thermal resistance values along with their associated uncertainties are plotted in Fig. 5. This indicates that among cold plates X, Y, and Z, cold plate Z has the maximum thermal resistance. Of the others, cold plate Y has the best thermal performance. The thermal resistance can be calculated using the following equation:

$$R_{th} = \frac{T_{heater} - T_{liq,in}}{q} \quad (1)$$

The hydraulic test of the cooling loops was performed at a constant coolant inlet temperature of 24 °C. The pressure drop includes the cooling loop, piping, and the quick disconnect with the fittings. As shown in Fig. 6(a), a comparison between the three cooling loops shows that cooling loops Y and X exhibit the lowest and maximum pressure drops, respectively. Fig. 6 (b) shows the results of the pressure drop of the quick disconnects and fittings at different flow rates. This experiment was conducted by looping the quick disconnect's inlet and outlet ports. It is noted from the results that the quick disconnects and fittings contribute most to the pressure drop values compared to the cooling loops.

3.2. TTVs case temperatures

Fig. 7 shows the case temperatures of the Type A and B heaters for the TTVs in each rack, where Rack A TTVs have type X cooling loops attached to them, Rack B has type Y, and Rack C has type Z. Each TTV reached a total power of 7.2 kW (800 W for Type A heaters and 133 W for Type B heaters), the coolant flow rate was 8 LPM/CL, and the coolant supply temperature was 32 °C. The temperatures of the heaters within a cooling loop exhibit variations due to the distribution of flow and the temperature of the supply coolant to the cold plates within it. For example, in cooling loop Y, the even-numbered Type A heaters have lower temperatures than the odd-numbered ones as the coolant enters the even-numbered cold plates, and then the preheated coolant enters the odd-numbered cold plate and exits the cooling loop via the common manifold, while for the Type B heaters, the coolant enters cold plate 1, then to 2 and flows to 3, then exits the cooling loop. Similar to this, the fluid enters cold plate 6 and goes via the 5th one and to the 4th cold plate before exiting the cooling loop.

3.3. Single rack test

Prior to testing the three racks for high-power testing with both CDUs, an initial assessment was performed under specific boundary conditions using a single CDU. This assessment involved loading only one rack with 6 TTVs. The total rack power reached 53 kW, the SAT was 15 °C with a coolant flow rate of 8 LPM/CL, and the measured total airflow from both CRAH units delivered to the cold aisle was 6144 cfm by using the flow hood. There is no control over the supply fluid temperature on the CDU side, as it relies mostly on the SAT and heat load. As shown in Fig. 8 (a), the HX fan speed was running steadily at 30% of its maximum speed until the power delivered from the power supply reached 30 kW. The fan speed started to increase and oscillate, trying to keep up by cooling the secondary fluid on the liquid side until it reached 100% by reaching the maximum input heat load. The secondary fluid temperature fluctuated as the fan speed oscillated, and the temperature reached a steady state as the fan speed reached 100%. It can also be noted from the results that the average heat removal from the liquid side at full fan speed is about 50 kW and the heat capture ratio by the fluid is 94%, while the remaining 6% is removed by air. Infrared (IR) images acquired during the experiment, as shown in Fig. 9, indicate a uniform distribution of air temperatures within the cold aisle. There is no significant evidence of recirculation of hot air to the cold aisle, which corroborates the average temperature readings obtained from the 22 temperature sensors positioned in front of the CDU in the cold aisle.

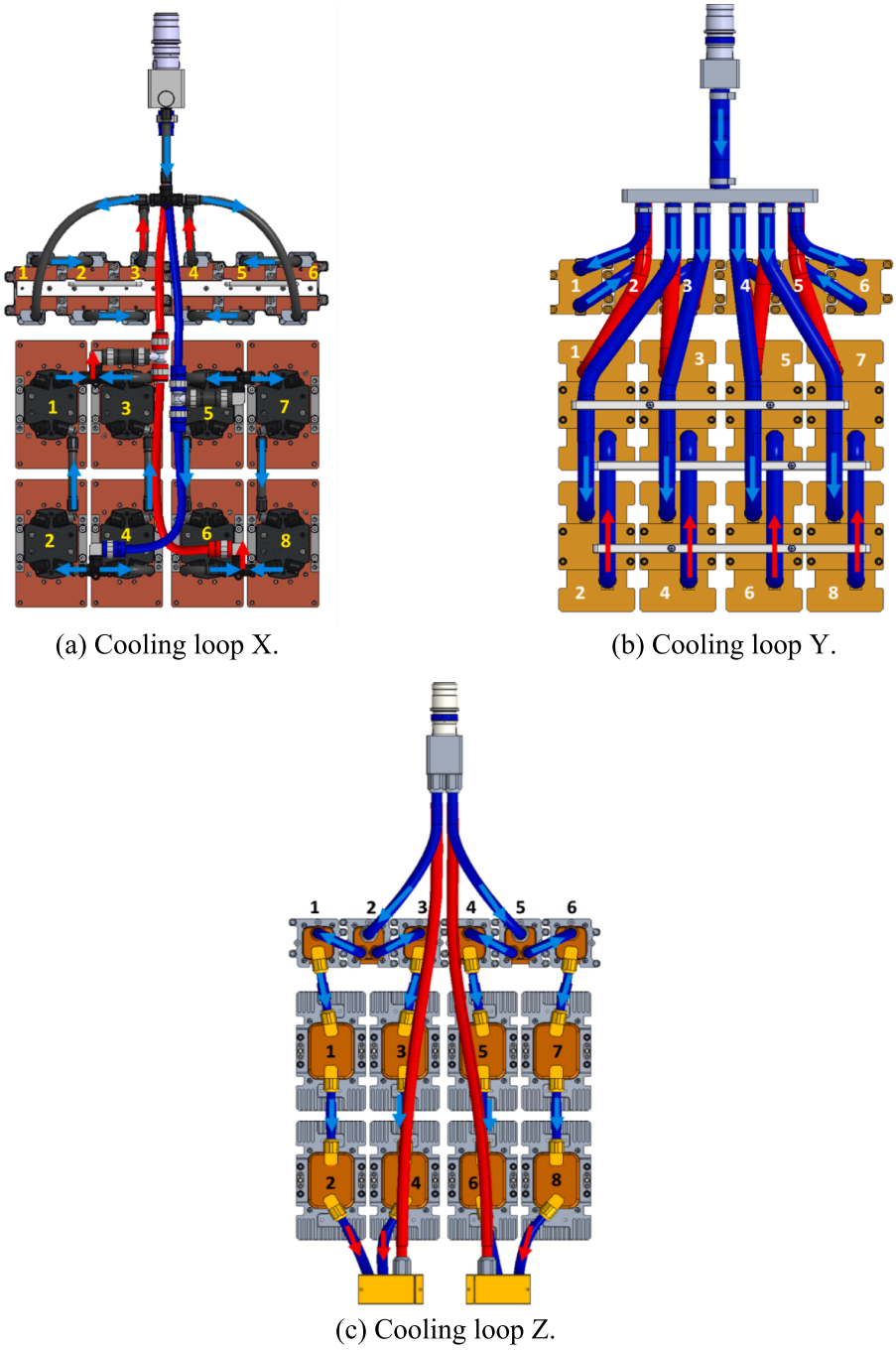

(a) Cooling loop X.

(b) Cooling loop Y.

(c) Cooling loop Z.

Fig. 4. Cooling loops configuration used in the test.

3.4. Multi-rack testing and CDUs performance

Two experiments were carried out employing both CDUs and the three racks. The initial experiment, labeled Test A, was conducted without utilizing blanking panels on the rear side of the racks within the cold aisle, which had 8 perforated tiles. The objective of this test was to assess the impact of air recirculation between the hot and cold aisle enclosures on the performance of the CDUs, as well as on the SFTs and SAT. The boundary conditions for this test were: the total power delivered to the racks was 82 kW (5.4 kW/TTV), there were 8 perforated tiles in the cold aisle, the SAT setpoint on the CRAHs was 13 °C, the measured airflow rate was 4670 cfm, and the fluid flow rate was 8 LPM/CL. A notable hot air recirculation from the hot aisle to the cold aisle was observed, contributing to an elevation in the cold aisle's SAT. This can be seen from the IR images taken during the experiment, as shown in Fig. 10.

Fig. 11 shows the experimental results of Test A, including the response parameters for both CDUs and the measured SAT. As the delivered power increases, the mixing between the hot and cold air increases, raising the SAT in the cold aisle from the setpoint, which was 13 °C, to 29 °C, which reflects on the fan speed of the CDUs and the SFTs. The fan speed oscillates before reaching 100% because of three major things. The first is insufficient airflow through the HX fans because there are only 8 perforated tiles in the cold aisle, as both HXs require airflow rated at 6650 CFM at 100% fan speed. The second is the increase in SAT, and the third one is the fan control type adapted by the unit.

To address this issue, blanking panels were installed on the rear side of the racks, and the number of perforated tiles within the cold aisle was

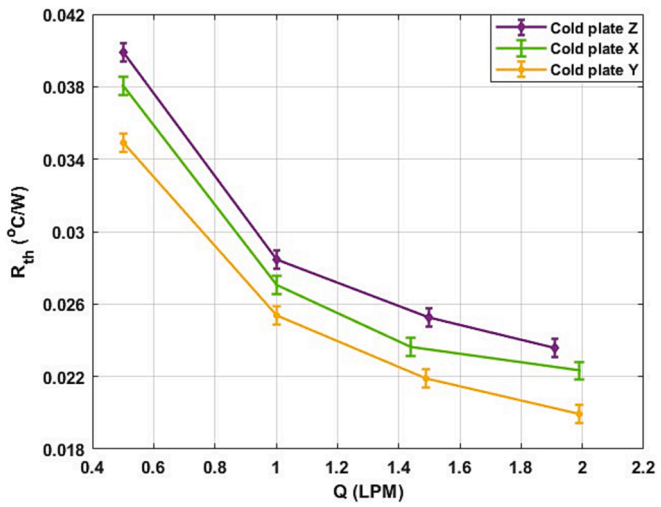

Fig. 5. Cold plate thermal resistance comparison for the three cooling loops used in the test at different flow rates.

increased to 18 tiles. This adjustment was made to guarantee an ample supply of cold air in the cold aisle [33]. Test B was conducted under these boundary conditions: the total power delivered to the racks was 128 kW (8.53 kW/TTV), there were 18 tiles in the cold aisle, the SAT setpoint on the CRAHs was 18 °C, the airflow rate from the CRAH units was 10,600 cfm, and the fluid flow rate was 8 LPM/CL. The results from the IR images as seen in Fig. 12 agree that the implementation of blanking panels and increasing the number of tiles assures uniform SAT, adequate airflow, and effectively prevents recirculation between the cold air and the hot air. The adjustments ensure a consistent temperature of the supplied fluid and a stable fan speed.

The results for Test B are shown in Fig. 13. The SAT in the cold aisle was constant around the setpoint at 18 °C during the experiment, as shown in Fig. 13 (b), and the fan speed oscillation is less compared to the fan speed in Test A because the hot air recirculation is limited and the SAT is more uniform in the cold aisle. A steady state was achieved at three stages of 10%, 50%, and 100% of total input power to observe the CDU's performance at low, medium, and maximum power. At 10% power, the CDUs' fans were running at a constant speed, and a 27.9 °C SFT was achieved after reaching a steady state. After that, the power was increased to 50% of the total power input, the fan speed started to increase in both units, and a steady SFT was achieved at 32.8 °C. After reaching maximum power, the fan speed went to 100%, and both units were running at full capacity, where a 39.3 °C SFT was achieved during steady-state operation.

The amount of heat picked up by the coolant was calculated for each TTV by using Eq. 2. The inlet and outlet coolant temperatures were measured at the cooling loop side by using calibrated thermistors, and the coolant flow rate entering each cooling loop was measured by using ultrasonic flow meters. Table 2 presents the measured data for coolant temperatures and flow rate with the calculated heat removal by the coolant for each TTV for the three racks for Test B.

$$q_{TTV} = \dot{m}_{TTV} C_{p\,PG25} \left(T_{Liq,out} - T_{Liq,in}\right) \tag{2}$$

Where q_{TTV} is the amount of heat carried by the coolant from the TTV, $\dot{m}_{TTV}$ is the mass flow rate of the coolant entering the cooling loop, and $C_{p_{PG25}}$ is the coolant specific heat.

Another important term to evaluate the CDU's HX thermal performance is the HX effectiveness (ε), which is determined as the ratio of the actual heat transfer to the maximum heat transfer that would happen if the fluid's temperature approached the SAT [34,35]. The following equations can be used to evaluate the effectiveness of HX and the heat removed by CDU:

$$\varepsilon = \frac{\mathbf{Actualheattransfer}}{\mathbf{Maximumpossibleheattransfer}} = \frac{\dot{\mathbf{m}}_{\mathbf{CDU}} \mathbf{C}_{\mathbf{p}_{\mathbf{PG25}}} \left(\mathbf{T}_{\mathbf{CDU,PG25in}} - \mathbf{T}_{\mathbf{CDU,PG25out}}\right)}{\left(\dot{\mathbf{m}}\mathbf{c}_{\mathbf{p}}\right)_{\mathbf{min}} \left(\mathbf{T}_{PG25,\mathbf{out}} - \mathbf{T}_{\mathbf{air,in}}\right)} \tag{3}$$

$$q_{actual} = q_{CDU} = \dot{m}_{CDU} C_{p_{PG25}} \left(T_{CDU,PG25in} - T_{CDU,PG25out}\right) \tag{4}$$

In Eq. (3), $\left(\dot{\mathbf{m}}\mathbf{c}_{\mathbf{p}}\right)_{\mathbf{min}}$ is the minimum value between air and PG25 when calculating the maximum possible heat transfer. Table 3 summarizes the data for both CDUs at maximum input power for Test B, and it shows that both units have approximately the same amount of heat removal and effectiveness as they are identical units. In addition, the heat capture ratio by the coolant can be found by dividing the heat removed by the CDUs by the total input power delivered by the power supplies, and it was found to be 93% while 7% was removed by air.

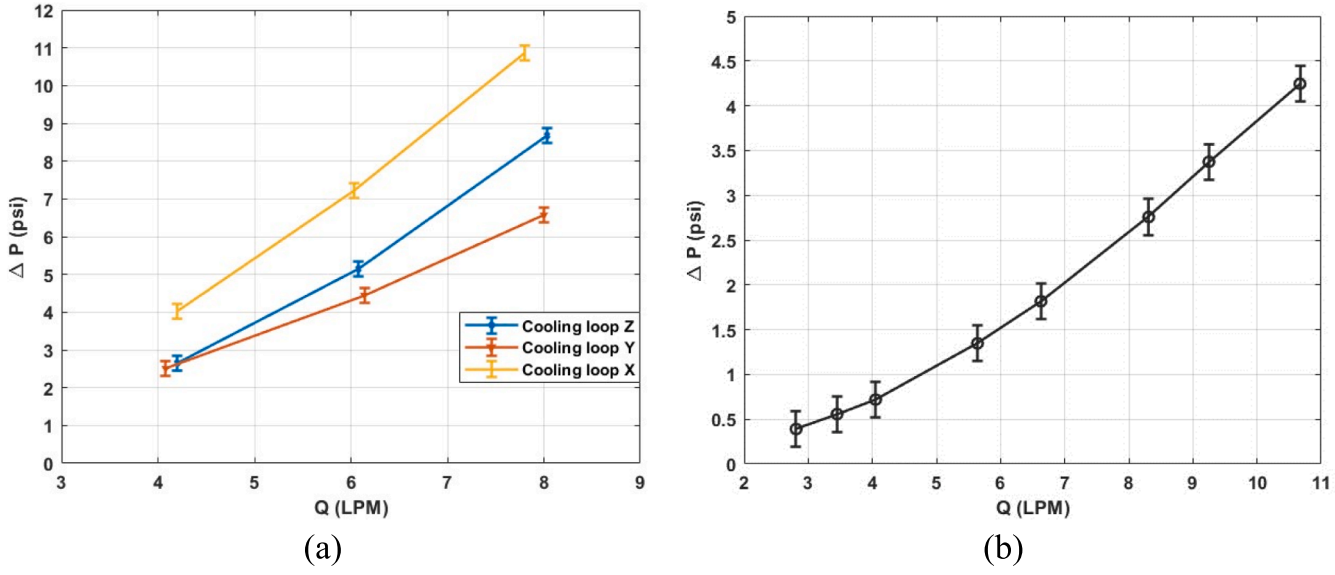

Fig. 6. (a) Pressure drop comparison for the three cooling loops at different flow rates. (b) Pressure drop of the quick disconnect.

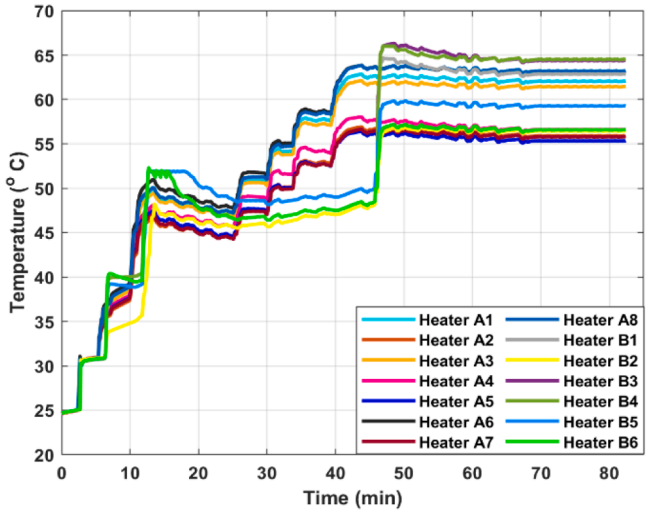

(a) Cooling loop X attached on the TTV.

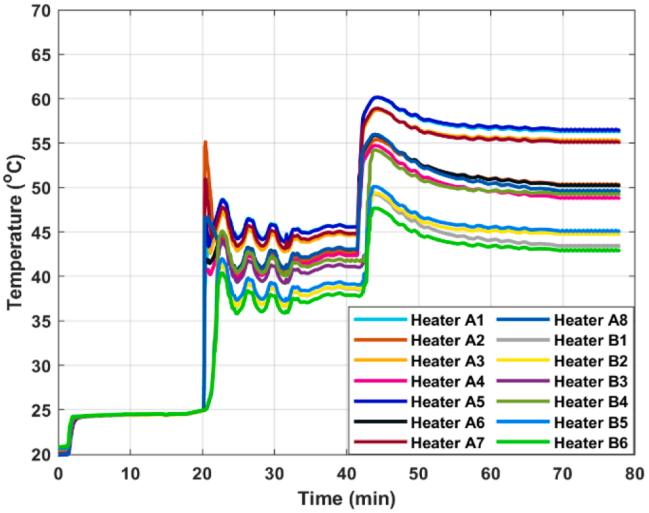

(b) Cooling loop Y attached on the TTV

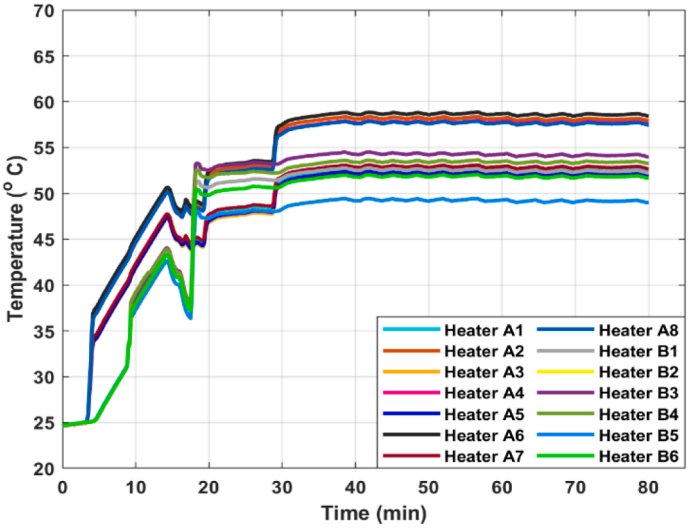

(c) Cooling loop Z attached on the TTV

Fig. 7. The case temperature of the type A and B heaters for each TTV with respect to time for the three types of cooling loops used in the experiment.

3.5. Uncertainty analysis

An essential stage in experimental research is uncertainty analysis, which evaluates and conveys the accuracy and reliability of the results. In order to provide a more thorough comprehension of the data, it measures the inherent variability and errors that are present in every measurement. Eq. (5) represents the collective uncertainty resulting from the contributions of uncertainties associated with each variable within the equation [36,37].

$$\omega_R = \sqrt{\left(\frac{\partial R}{\partial X_1}\omega_1\right)^2 + \left(\frac{\partial R}{\partial X_2}\omega_2\right)^2 + \cdots + \left(\frac{\partial R}{\partial X_n}\omega_n\right)^2} \tag{5}$$

Where ω_R represents the uncertainty in the final result, while $\omega_1, \omega_2, \cdots, \omega_n$ represent the uncertainties associated with the independent variables, and R is the measured or calculated data that might depend on other variables, for example, the thermal resistance, which depends on the case temperature, coolant inlet temperature, and the total power. Table 4 presents all the uncertainties associated with the data that were measured and calculated in the preceding sections.

4. Conclusion

This study introduces an innovative experimental framework aimed at assessing the feasibility of incorporating single-phase liquid cooling for high power-density DCs through the utilization of in-row liquid-to-air CDUs. The key outcomes of this study are outlined as follows:

- Initially, a comprehensive evaluation of the thermohydraulic performance of various cooling loops was conducted, revealing that cooling loop Y demonstrated superior thermal and hydraulic efficiency compared to the alternatives. This loop exhibited a thermal resistance of 0.0198 °C/W and a pressure drop of 6.55 psi.
- A test was conducted on a single rack with a cooling distribution unit (CDU) operating at lower and higher power levels. The CDU effectively managed heat removal in both tests. However, during the higher power test with multiple racks, issues of air recirculation were observed due to open rack backs.
- To address the air recirculation problem, blanking panels were added to the rear of the racks. This adjustment was followed by another test at even higher power, where the panels successfully prevented air recirculation and maintained consistent temperatures in the cold aisle. The CDU's cooling capacity and the effectiveness of heat

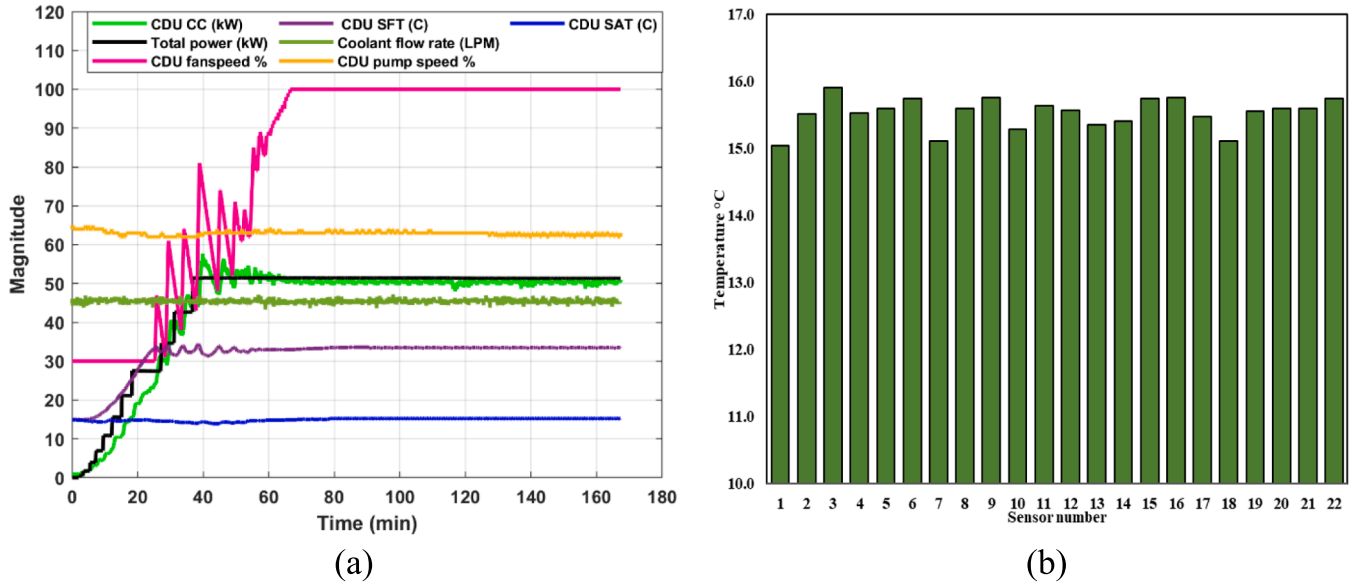

Fig. 8. (a) CDU Cooling capacity comparison with total power delivered by power supply. (b) Cold air average temperatures in the cold aisle.

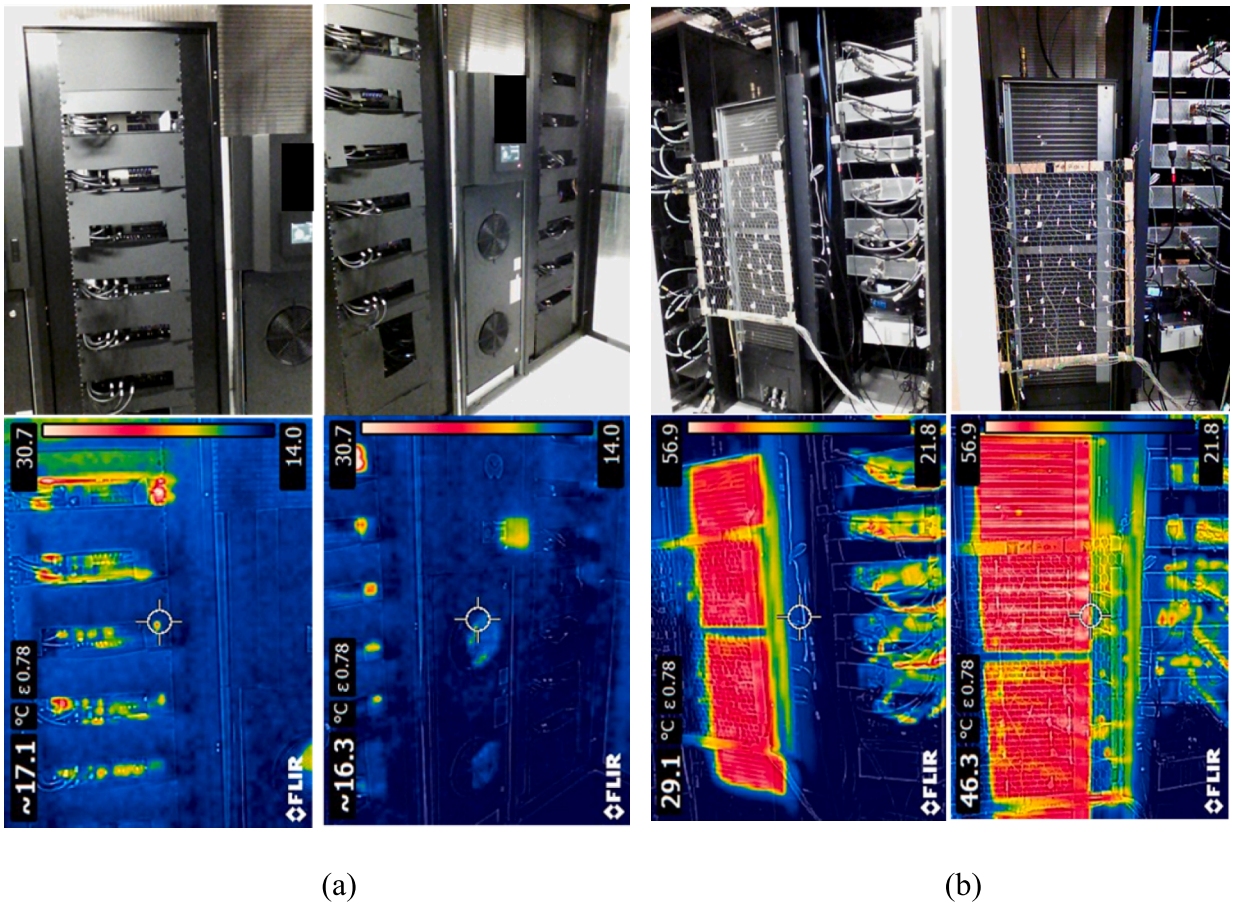

Fig. 9. (a) IR images in the cold aisle. (b) IR images in the hot aisle.

exchangers (HX) were also measured and calculated. The liquid phase displayed a remarkable ability to handle a significant portion of the heat load.

- In summary, this study conclusively establishes the efficacy of implementing liquid-to-air (L2A) cooling methodologies within data centers, effectively addressing the intricate challenges posed by escalating IT equipment power densities. The findings underscore the potential of this approach to revolutionize data center cooling strategies and enhance overall operational efficiency.

Fig. 10. IR images taken during the experiment in the cold aisle before installing the blanking panels.

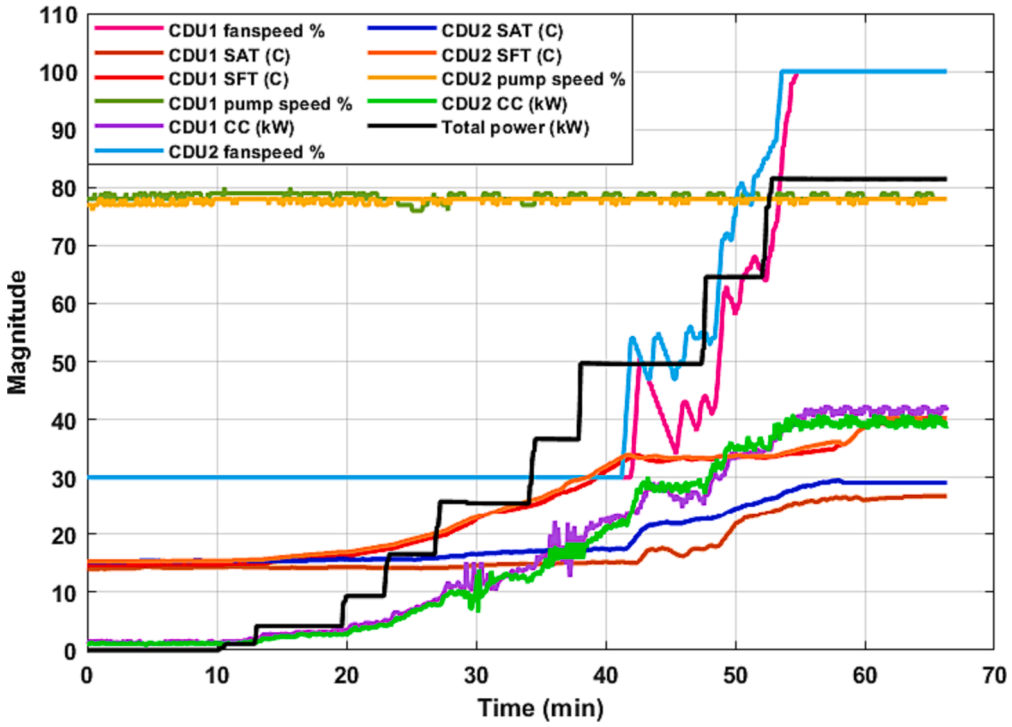

Fig. 11. Results of Test A.

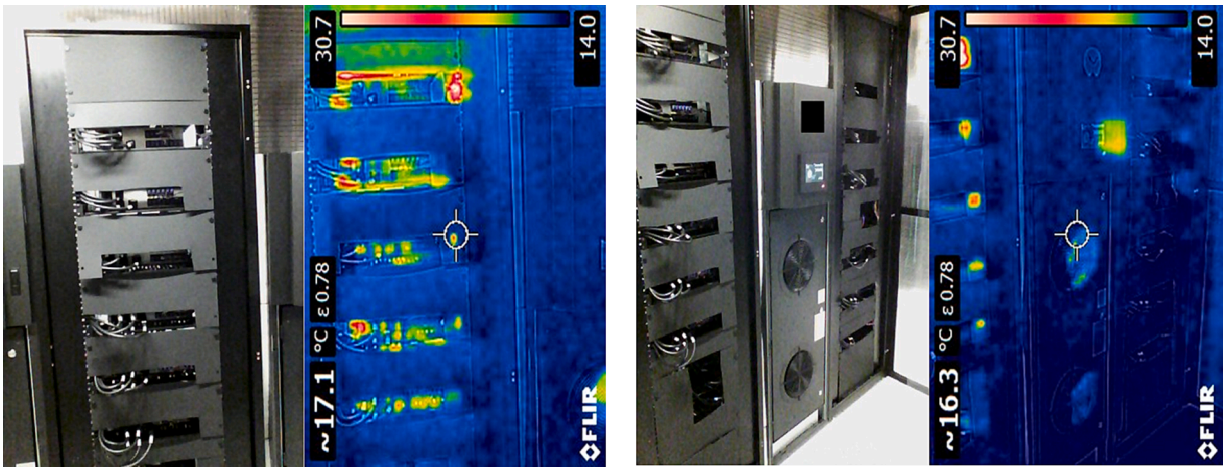

Fig. 12. IR images taken during the experiment in the cold aisle after installing the blanking panels.

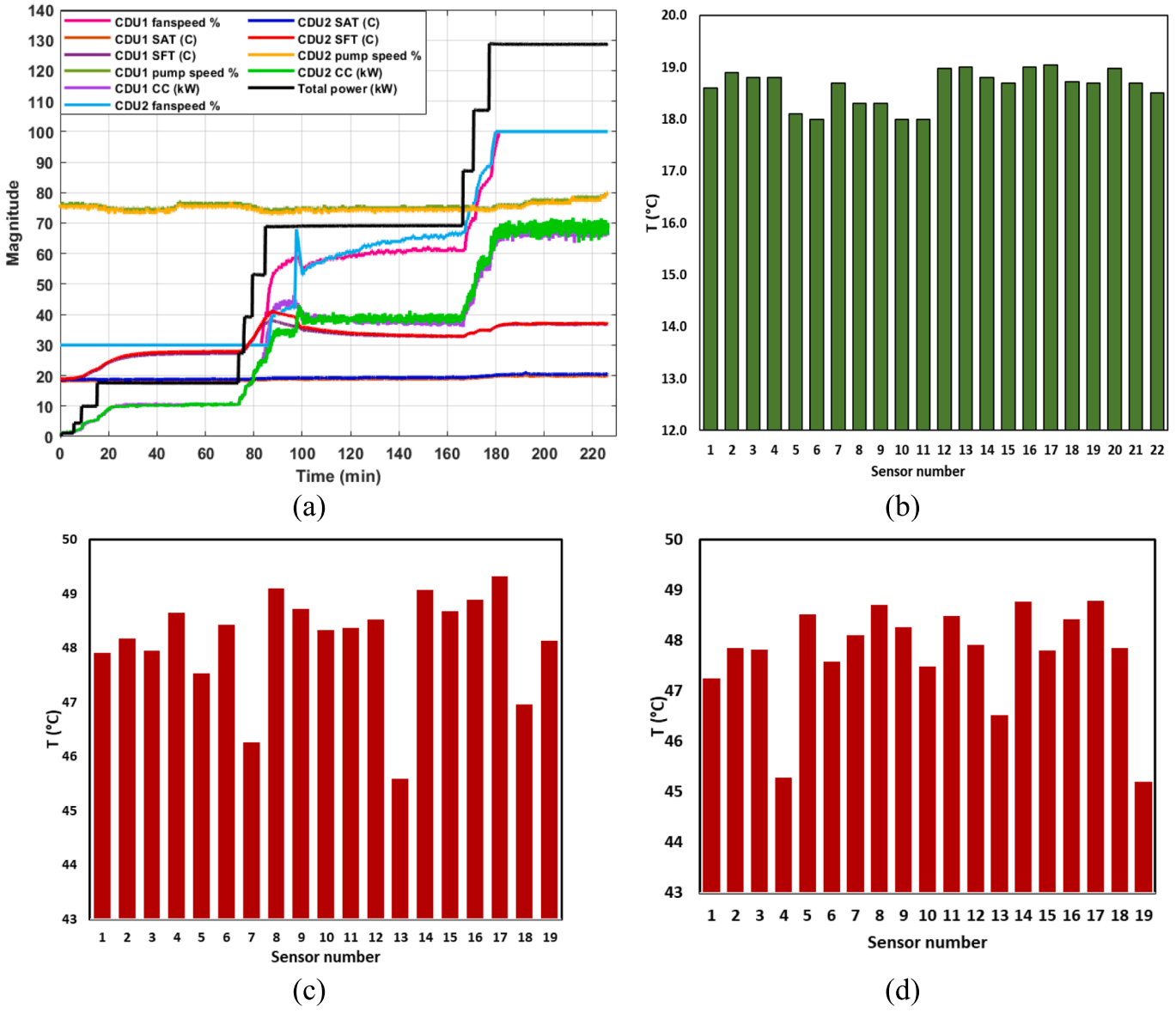

Fig. 13. Results of Test B (a) Response parameters of both CDUs. (b) Average SAT readings in the cold aisle. (c) Average hot air temperature on CDU 1 side. (d) Average hot air temperature on CDU 2 side.

Table 2
The calculated heat removal data for the TTVs in Test B with TTVs cooling loop flow rate and inlet and outlet coolant temperatures.

Rack A					
	TTV1	**TTV2**	**TTV3**	**TTV4**	**TTV5**
T_{in} (°C)	38.87	39.14	39.26	39.25	39.12
T_{out} (°C)	53.5	53.54	53.2	54.04	53.54
Q_{PG25} (LPM)	8.11	8.15	8.2	7.97	8.05
q (kW)	7.94	7.85	7.65	7.88	7.77
Rack B					
	TTV1	**TTV2**	**TTV3**	**TTV4**	**TTV5**
T_{in} (°C)	39.78	39.82	39.84	39.66	39.27
T_{out} (°C)	54.9	54.91	54.39	54.88	54.31
Q_{PG25} (LPM)	7.92	8	8.1	7.95	8.04
q (kW)	8.01	8.07	7.88	8.09	8.09
Rack C					
	TTV1	**TTV2**	**TTV3**	**TTV4**	**TTV5**
T_{in} (°C)	39.14	39.25	39.09	39.13	39.22
T_{out} (°C)	53.74	53.98	53.42	53.19	53.72
Q_{PG25} (LPM)	8.05	8.07	8.2	8.23	8.07
q (kW)	7.86	7.95	7.86	7.74	7.83

Table 3
CDUs response parameters for Test B.

	CDU 1	**CDU 2**
SAT (°C)	18.6	18.8
RAT (°C)	48	47.8
SFT (°C)	39.15	39.53
RFT (°C)	53.8	54.29
Coolant flow rate (LPM)	59.95	59.1
Air flow rate (m^3/s)	1.641	1.655
Actual heat transfer (kW)	58.87	58.5
Maximum heat transfer (kW)	70.19	71.31
ε	0.83	0.82

Declaration of Competing Interest

The authors declare that they have no known competing financial interests or personal relationships that could have appeared to influence the work reported in this paper.

Table 4
Uncertainties of the measured and calculated parameters.

	Sensor accuracy	Uncertainty
Temperature (°C)	±0.2 °C	0.2 °C
Pressure drop (°psi)	±0.145 psi	±0.2 psi
Input power (kW)	±0.1 %	±0.1 %
Coolant flow rate (LPM)	±0.003 ml/min	±0.003 ml/min
Air flow rate (m^3/s)	±3 %	±3 %
Thermal resistance (W/°C)	–	±0.0005 W/°C
Actual heat transfer (kW)	–	±0.15 kW
Effectiveness	–	±0.009

Data availability

Data will be made available on request.

Acknowledgment

We would like to acknowledge NVIDIA. This work is supported by NVIDIA and NSF IUCRC Award No. IIIP-2209776 and MRI Award No. CNS1040666.

References

[1] K. W. Yan, P. Y. Lin, S. L. Kuo, Thermal Challenges for HPC 3DFabricTMPackages and Systems, IEEE International Reliability Physics Symposium Proceedings, vol. 2022-March, pp. 4C11-4C16, 2022, doi: 10.1109/IRPS48227.2022.9764572.
[2] I. Sauciuc, G. Chrysler, R. Mahajan, M. Szleper, Air-cooling extension - Performance limits for processor cooling applications, Annual IEEE Semiconductor Thermal Measurement and Management Symposium, pp. 74–81, 2003, doi: 10.1109/STHERM.2003.1194342.
[3] J. Broughton, V. Smet, R.R. Tummala, Y.K. Joshi, Review of thermal packaging technologies for automotive power electronics for traction purposes, J. Electron. Packaging, Trans. ASME 140 (4) (2018) Dec, https://doi.org/10.1115/1.4040828/366154.
[4] H. Y. Zhang, D. Pinjala, P.S. Teo, Thermal management of high power dissipation electronic packages: From air cooling to liquid cooling, Proceedings of 5th Electronics Packaging Technology Conference, EPTC 2003, pp. 620–625, 2003, doi: 10.1109/EPTC.2003.1271593.
[5] G.D. Chethana, B.S. Gowda, Thermal management of air and liquid cooled data centres: A review, Mater. Today Proc 45 (Jan. 2021) 145–149, https://doi.org/10.1016/J.MATPR.2020.10.396.
[6] M.K. Sung, I. Mudawar, Single-Phase and two-phase hybrid cooling schemes for high-heat-flux thermal management of defense electronics, J. Electron. Packaging, Trans. ASME 131 (2) (Jun. 2009) 0210131–02101310, https://doi.org/10.1115/1.3111253/466145.
[7] A.C. Kheirabadi, D. Groulx, Experimental evaluation of a thermal contact liquid cooling system for server electronics, Appl. Therm. Eng. 129 (Jan. 2018) 1010–1025, https://doi.org/10.1016/J.APPLTHERMALENG.2017.10.098.
[8] Y.A. Manaserh, A.R. Gharaibeh, M.I. Tradat, S. Rangarajan, B.G. Sammakia, H.A. Alissa, Multi-objective optimization of 3D printed liquid cooled heat sink with guide vanes for targeting hotspots in high heat flux electronics, Int. J. Heat Mass Transf., p. 122287, Dec. 2021, doi: 10.1016/J.IJHEATMASSTRANSFER.2021.122287.
[9] A.R. Gharaibeh, Y.M. Manaserh, M.I. Tradat, F.W. AlShatnawi, S.N. Schiffres, B.G. Sammakia, Using a Multi-Inlet/Outlet Manifold to Improve Heat Transfer and Flow Distribution of a Pin Fin Heat Sink, J. Electron. Packag., vol. 144, no. 3, Sep. 2022, doi: 10.1115/1.4054461.
[10] C.H. Hoang, et al., Impact of fin geometry and surface roughness on performance of an impingement two-phase cooling heat sink, Appl. Therm. Eng. 198 (Nov. 2021), 117453, https://doi.org/10.1016/J.APPLTHERMALENG.2021.117453.
[11] J.M. Shah, K. Padmanaban, H. Singh, S. Duraisamy Asokan, S. Saini, D. Agonafer, Evaluating the Reliability of Passive Server Components for Single-Phase Immersion Cooling, J. Electron. Packag., vol. 144, no. 2, Jun. 2022, doi: 10.1115/1.4052536.
[12] M. Jalili *et al.*, Cost-efficient overclocking in immersion-cooled datacenters, Proc Int Symp Comput Archit, vol. 2021-June, pp. 623–636, Jun. 2021, doi: 10.1109/ISCA52012.2021.00055.
[13] R. Schmidt, M. Steinke, A. S.-A. Journal, and undefined 2019, Moderating the Impact of Integrating Water-Cooled Servers Into Data Centers., airah.org.au, Accessed: Dec. 02, 2022. [Online]. Available: https://www.airah.org.au/Content_Files/EcoLibrium/2021/10-21-Eco-technical-paper.pdf.
[14] M.J. Ellsworth, L.A. Campbell, R.E. Simons, M.K. Iyengar, R.R. Schmidt, R.C. Chu, The evolution of water cooling for IBM large server systems: Back to the future, in: 2008 11th IEEE Intersociety Conference on Thermal and Thermomechanical Phenomena in Electronic Systems, 2008, pp. 266–274, https://doi.org/10.1109/ITHERM.2008.4544279.
[15] R. Schmidt, M. Iyengar, D. Porter, … G. W.-2010 12th I., and undefined 2010, Open side car heat exchanger that removes entire server heat load without any added fan power, *ieeexplore.ieee.org*, Accessed: Jun. 28, 2023. [Online]. Available: https://ieeexplore.ieee.org/abstract/document/5501423/?casa_token=CCCi1PsOjVAAAAAA:at8SWiOd2YdZ_LOjxcIGiSkLi8Dbth8W8tNt87q1qIWLayYWCFtbFx2p6DWx4xBumL1mT_szdfo.
[16] U. Chowdhury, W. Hendrix, T. Craft, W. James, A. Sutaria, and D. Agonafer, Optimal design and modeling of server cabinets with in-row coolers and air conditioning units in a modular data center, asmedigitalcollection.asme.org, 2019, Accessed: Apr. 15, 2023. [Online]. Available: https://asmedigitalcollection.asme.org/InterPACK/proceedings-abstract/InterPACK2019/V001T02A009/1071704?casa_token=g0Za9sKN9ucAAAAA:PgUSeqlPRDpyocqKdSYcYDiR2VnFVdUzK8Dipz4dYK8Yl_fe4Zb19YDUqew-eInQXmcHMw6KbA.
[17] T. Gao, B. G. Sammakia, J. Geer, B. Murray, R. Tipton, R. Schmidt, Comparative Analysis of Different In Row Cooler Management Configurations in a Hybrid Cooling Data Center, ASME 2015 International Technical Conference and Exhibition on Packaging and Integration of Electronic and Photonic Microsystems, InterPACK 2015, collocated with the ASME 2015 13th International Conference on Nanochannels, Microchannels, and Minichannels, vol. 1, Nov. 2015, doi: 10.1115/IPACK2015-48069.
[18] T. Gao, H. Tang, Y. Cui, Z. Luo, A Test Study of Technology Cooling Loop in a Liquid Cooling System, in Proceedings of the 17th InterSociety Conference on Thermal and Thermomechanical Phenomena in Electronic Systems, ITherm 2018, Institute of Electrical and Electronics Engineers Inc., Jul. 2018, pp. 740–747. doi: 10.1109/ITHERM.2018.8419519.
[19] M. Hnayno, A. Chehade, H. Klaba, … H. B.-A. T., and undefined 2022, Performance analysis of new liquid cooling topology and its impact on data centres, Elsevier, Accessed: Jun. 28, 2023. [Online]. Available: https://www.sciencedirect.com/science/article/pii/S1359431122006779.
[20] R. Udakeri, V. Mulay, D. A.-2008 T. Annual, and undefined 2008, Comparison of overhead supply and underfloor supply with rear heat exchanger in high density data center clusters, ieeexplore.ieee.org, Accessed: Jun. 28, 2023. [Online]. Available: https://ieeexplore.ieee.org/abstract/document/4509385/?casa_token=w61ReutdGuIAAAAA:65wrEak9XOGnPZqp1Mg_U9z8lek2gZXXfayWwN5PnltmsLJ7DjWli-SfKYqcW1XqM1GWifyXiOg.
[21] A. Capozzoli, G. Primiceri, Cooling systems in data centers: State of art and emerging technologies, in Energy Procedia Elsevier Ltd (Dec. 2015) 484–493, https://doi.org/10.1016/j.egypro.2015.12.168.
[22] P. Shahi, S. Saini, P. Bansode, D. Agonafer, A comparative study of energy savings in a liquid-cooled server by dynamic control of coolant flow rate at server level, IEEE Trans Compon Packaging Manuf Technol 11 (4) (Apr. 2021) 616–624, https://doi.org/10.1109/TCPMT.2021.3067045.
[23] S. Nada, R. El-Zoheiry, … M. E.-C. S. in T., and undefined 2021, Experimental investigation of hydrothermal characteristics of data center servers' liquid cooling system for different flow configurations and geometric, Elsevier, Accessed: Jun. 28, 2023. [Online]. Available: https://www.sciencedirect.com/science/article/pii/S2214157X21004391.
[24] M. Iyengar et al., Server liquid cooling with chiller-less data center design to enable significant energy savings, Annual IEEE Semiconductor Thermal Measurement and Management Symposium, pp. 212–223, 2012, doi: 10.1109/STHERM.2012.6188851.
[25] S. Zimmermann, I. Meijer, M.K. Tiwari, S. Paredes, B. Michel, D. Poulikakos, Aquasar: A hot water cooled data center with direct energy reuse, Energy 43 (1) (Jul. 2012) 237–245, https://doi.org/10.1016/J.ENERGY.2012.04.037.
[26] M. Iyengar et al., Server liquid cooling with chiller-less data center design to enable significant energy savings, in: Annual IEEE Semiconductor Thermal Measurement and Management Symposium, 2012, pp. 212–223. doi: 10.1109/STHERM.2012.6188851.
[27] B.A. Rubenstein, R. Zeighami, R. Lankston, E. Peterson, Hybrid cooled data center using above ambient liquid cooling, in: in 2010 12th IEEE Intersociety Conference on Thermal and Thermomechanical Phenomena in Electronic Systems, ITherm 2010, 2010, https://doi.org/10.1109/ITHERM.2010.5501426.
[28] D.C. Hwang, V.P. Manno, M. Hodes, G.J. Chan, Energy savings achievable through liquid cooling: A rack level case study, in: 2010 12th IEEE Intersociety Conference on Thermal and Thermomechanical Phenomena in Electronic Systems, ITherm 2010, 2010. doi: 10.1109/ITHERM.2010.5501419.
[29] B. Watson, V.K. Venkiteswaran, Universal Cooling of Data Centres: A CFD Analysis, in Energy Procedia Elsevier Ltd (2017) 2711–2720, https://doi.org/10.1016/j.egypro.2017.12.215.
[30] A. Heydari *et al.*, "Liquid to liquid cooling for high heat density liquid cooled data centers ipack2022-97416," 2022. [Online]. Available: http://asmedigitalcollection.asme.org/InterPACK/proceedings-pdf/InterPACK2022/86557/V001T01A007/6957569/v001t01a007-ipack2022-97416.pdf.
[31] A. Heydari *et* al., Liquid to Air Cooling for High Heat Density Liquid Cooled Data Centers, Proceedings of ASME 2022 International Technical Conference and Exhibition on Packaging and Integration of Electronic and Photonic Microsystems, InterPACK 2022, Dec. 2022, doi: 10.1115/IPACK2022-97386.
[32] A. Heydari et al., Guidelines and Experimental Hydraulic performance Evaluation for Single-Phase CDUs Under Steady and Transient Events, InterSociety Conference on Thermal and Thermomechanical Phenomena in Electronic Systems, ITHERM, vol. 2023-May, 2023, doi: 10.1109/ITHERM55368.2023.10177633.
[33] V.K. Arghode, Y. Joshi, Modeling strategies for air flow through perforated tiles in a data center, IEEE Trans Compon Packaging Manuf Technol 3 (5) (2013) 800–810, https://doi.org/10.1109/TCPMT.2013.2251058.
[34] M. Kassai, C. S.-B. S. Engineering, and undefined 2015, Performance investigation of liquid-to-air membrane energy exchanger under low solution/air heat capacity

rates ratio conditions, journals.sagepub.com, vol. 36, no. 5, pp. 535–545, Sep. 2015, doi: 10.1177/0143624414564445.
[35] Y.M. Manaserh, M.I. Tradat, A.R. Gharaibeh, B.G. Sammakia, R. Tipton, Shifting to energy efficient hybrid cooled data centers using novel embedded floor tiles heat exchangers, Energy Convers Manag 247 (Nov. 2021), 114762, https://doi.org/10.1016/J.ENCONMAN.2021.114762.
[36] J. Holman, Experimental Methods for Engineers EIGHTH EDITION, 2021, Accessed: Oct. 28, 2023. [Online]. Available: http://debracollege.dspaces.org/handle/123456789/560.
[37] S. Kiwan, Q.R. Soud, Experimental investigation of the thermal performance of a sand-basalt heat storage system for beam-down solar concentrators, Case Stud. Therm. Eng. 19 (Jun. 2020), https://doi.org/10.1016/j.csite.2020.100609.